Damage-Fragmentation Transition: Size Effect and Scaling Behavior for Impact Fragmentation of Slender Projectiles

Sreten Mastilovic*

Union – Nikola Tesla University, Cara Dusana 62-64, Belgrade, Serbia

ABSTRACT: The focus of the present article is on the size effect of a transition region from the damaged to the fragmented phase in impact-induced breakup of a slender projectile. Molecular dynamics simulations of the classic ballistic Taylor test are performed with a simple generic model to explore an extended low-energy range. In the simulation setup, flat-ended, monocrystalline, nanoscale projectiles, with a fixed aspect ratio but ten different diameters, collide perpendicularly with a rough rigid wall. With gradually increasing impact energy, a non-negligible projectile disintegration eventually takes place and is identified with the damage-fragmentation phase transition. These atomistic simulations offer an indispensable tool to gain an insight into damage evolution in the neighborhood of the damage-fragmentation transition resulting in the occurrence of fragmentation at the critical point. A finite size scaling analysis of the average fragment mass is carried out to determine critical exponents and dependence of the critical striking velocity upon the slender projectile's diameter.

KEY WORDS: impact fragmentation, slender projectiles, size effect, scaling laws, phase transition, atomistic simulations

INTRODUCTION

A sudden mechanical disintegration of solids is a widespread process inherent to many natural phenomena and industrial technologies. It is an irreversible, nonlinear, and far-from-equilibrium phenomenon difficult to investigate with the traditional methods of continuum mechanics (e.g., Krajcinovic, 1996; Wu et al., 2014). An example is the rigid-anvil collision, addressed in this study, that triggers a sequence of

* E-mail: smastilovic@fgm.edu.rs

operating deformation and damage mechanisms with different characteristic thresholds and time scales. The integration of these mechanisms results in dynamic response of a material typically characterized by steep deformation and thermal gradients (e.g., Mastilovic, 2016), which may—given sufficient impact energy—eventually lead to a sequential fracture and culminate in energetic ejection of fragment debris. The more-or-less abrupt transition from damage accumulation to fragmentation in low-energy collisions is a complex and fascinating phenomenon explored in a number of articles over the last 15 years (Kun and Herrmann, 1999; Åström et al., 2000; Herrman et al., 2006; Carmona et al., 2008; Sator and Hietala. 2010; Timár et al., 2012).

Phase transition is, in condensed matter physics, defined as the transition between two phases of matter whose signature is "a singularity or discontinuity in some observable quantity" (Chaikin and Lubensky, 1995). The mean-field modeling of the phase transition is based on concepts of the correlation length and the order parameter (Krajcinovic, 1996). The former is, in damage mechanics, identified with the length (or mass) of correlated microcrack forming a shear band, while the later, separating an ordered phase from disordered phase, is commonly identified with the effective stiffness. The concept of *fragmentation* phase transition originated in nuclear physics (e.g., Campi 1988; Sá Martins de Oliveira, 1998). Kun and Herrmann in their pioneering investigation (1999) applied the same conceptual approach on two-dimensional (2D) mechanical particle collisions, studied the possible mechanism of the damage-fragmentation (D-F) transition and offered numerical evidence of the existence of criticality in low-energy fragmentation at a single value of impact energy clearly distinguishing the damaged and fragmented states. The damaged state is statistically homogeneous (or translation invariant) while the fragmented state is, by definition, heterogeneous on macroscopic scale due to the presence of the system-spanning faults that yield fragments. Thus, similarly to the percolation based ideas developed originally in nuclear physics, Kun and Herrmann (1999) suggested existence of the continuous phase transition with the imparted energy as the natural control parameter and the size of the largest fragment as the order parameter. Interestingly, they also clearly identified the critical point with the position of the maximum value of the ratio of the damage energy and the impact energy. (The same authors and their collaborators (Carmona et al., 2008; Timár et al., 2012) extended this approach to collisions of spheres and investigated in detail the damage and fracture mechanisms unique to three-dimensional (3D) fragmentation.) Åström et al. (2000) also used a 2D model of computational mechanics of discontinua and statistical arguments to investigate the threshold of instantaneous fragmentation and explore the nature of the suggested fragmentation criticality. They confirmed that impact fragmentation indeed becomes critical at a

well-defined impact energy preceded by relatively modest damage accumulation prior to that critical point. The critical point of the D-F phase transition was identified with the striking velocity corresponding to the maximum value of the average fragment mass (Timár et al, 2012). Substantial literature exists in which the scaling behavior in dynamic fragmentation was investigated both experimentally and theoretically. Diehl et al. (2000) studied scaling behavior in explosive fragmentation of generic LJ (Lennard-Jones) systems with emphasis on the initial temperature. Damage in impact fragmentation was investigated by Sator and coworkers (2008, 2010) by using a simple MD (molecular dynamics) model of a point impact. A discrete element model was used by Timár et al (2012) to study the scaling laws for impact fragmentation of spherical solids upon a hard wall collision. The D-F transition was also investigated experimentally; for example, by Andrews and Kim (1998), Katsuragi et al. (2003, 2004) and Moukarzel et al. (2007).

The objective of the present study is to apply the above mentioned concepts to the impact fragmentation of *slender* projectiles with emphasis on the size effect of the D-F phase transition. The MD simulation results are used to explore the dependence of selected fragment statistics upon the striking velocity and to search for the typical critical-behavior features and the transition order paramater(s). The D-F transition is investigated using the time-honored mathematical tools of percolation theory to capture the size effect and determine the exponents and the limits of applicability of the ubiquitous power-law scaling expressions.

SIMULATION METHOD

MD is used extensively to investigate the fragmentation under various types of extreme loading conditions by the high-resolution virtual (computational) testing (Holian and Grady, 1988; Diehl et al., 2000; Sator and Hietala, 2010; Mastilovic, 2015). The present study is limited to the traditional MD simulation technique in 2D in which the dynamic state of the atomic system is defined by laws of classical mechanics with atomic motions being uniquely determined by an empirical potential. The fragmentation model proposed is, therefore, general since it aims to capture the underlying features of the investigated phenomenon. The model is described in detail in a preceding study (Mastilovic, 2016), thus, a succinct summary is deemed sufficient herein.

A monatomic system, mimicking a monocrystalline flat-nosed (rectangular) projectile, is comprised of N atoms of equal masses m_0 that form an ideal triangular lattice and interact with their nearest neighbors according to the LJ potential. MD simulations are carried out with three LJ model parameters set in the preceding studies (Mastilovic, 2015, 2016) to match, as close as possible, physical properties of tungsten ($_{74}$W): the atomic mass $m_0 = 3.1\times10^{-25}$ kg (183.85 u), the atomic radius 1.4 Å ($\equiv r_0/2$ where r_0 is the equilibrium interatomic distance), and the depth of the potential well $\varepsilon = 7.5\times10^{-20}$ J. The simulations are performed for 10 different projectile sizes that share the common aspect ratio, $\lambda\approx7.5$. (The projectile diameters, d, are defined in units of the equilibrium atomic distance, r_0, throughout the present article, $\bar{d} = d/r_0$.) The coordination number of bulk atoms in the reference configuration is six and the potential energy per atom is, depending of the model size, somewhat in excess of the bulk value (-3ε) due to the surface effects. The Cauchy problem is solved numerically by using the neighbor-list method and the Verlet algorithm (Verlet, 1967; Allen and Tildesley, 1996) with the time step of the order of femtoseconds (Mastilovic, 2016). The extremely small time step, necessitated by the high power of the simulated events, makes the simulations painstakingly time-consuming even for the relatively small model size utilized herein due to the recognized difficulty to reach an equilibrium state (Holian and Grady, 1988; Åström et al., 2000; Mastilovic, 2015). The present MD simulations are interrupted when the steady-state fragment mass distribution is asymptotically reached, which also coincides with thermal equilibrium.[1] The small scale examination of the high-velocity short-duration events of violent nature, such as impact fragmentation, is perfectly suited to the virtual experiments by methods of the computational mechanics of discontinua (Mastilovic and Rinaldi, 2014). The conversion of simulation data generated at the nanoscale level (atomic positions and velocities, and interatomic forces) to macroscopic observables (temperature, stress and strain) is firmly established nowadays (e.g., Hoover, 1985; Holian et al., 1995; Zhou, 2003; Buehler, 2008; Mastilovic and Rinaldi, 2014; Mastilovic, 2016).

The distribution of fragment masses is identified in the final state following the normal impact of a slender deformable LJ projectile with a rigid target. The projectile is in its initial condition a perfect crystal

[1] The largest simulations took three months of CPU time of PC with Intel® i5-4440 3.10 GHz processor. Since the computational cost for MD simulations scales typically with the square of the total number of atoms (Dongarra et al., 2008), the extension of the present investigation to 3D geometry would require an increase of execution time of the order of $\bar{d}^2/2$. Obviously, such computational effort would necessitate both the more powerful hardware than the one used in the present study and the parallel computing.

prepared at zero temperature (free of any quenched disorder and thermal vibratory oscillations). For the continuum-scale ballistic Taylor tests at moderate striking velocities, the anvil surface preparation and appropriate lubrication are very important for the experiment outcome. In the current MD model, a set of immovable atoms, which exerts a compressive dynamic load on the impacting projectile without any numerical artifices mimicking lubrication, represents a rough rigid-target contact surface. In a hindsight, it may be preferable to use the frictionless target (e.g., Behera et al., 2005) for the study of the D-F transition (by definition a critical phenomenon associated with the *low-energy* impacts) to promote the fragmentation in the neighborhood of the critical point by preventing that the target "wetting" (the thin elongated fragments, distinctly visible in Figure 1, which combine relatively small momentum with comparably large rough-wall adhesion) hinders the lateral mass transfer. Furthermore, the initial thermal equilibration at any given temperature would offer an opportunity to perform repeated statistical realizations of the Taylor test at any given striking velocity.

The link between two atoms ruptures when their interatomic distance exceeds the predetermined critical value $R \approx 1.7\, r_0$. This cut-off interatomic distance is selected to be between the first and second nearest neighbors in the reference configuration. A fragment is defined as a self-bound cluster of atoms with interatomic distance less than the cut-off distance ($r_{ij} \leq R$) in a sequential atom-by-atom search for the nearest neighbors (Mastilovic, 2015, 2016).

OBSERVATIONS AND DISCUSSION

The present investigation of the normal impact fragmentation of slender projectiles is focused on the size effect of the transition from damaged to the fragmented deformation phase. According to the MD simulation results, at striking velocities corresponding to an extended transonic range below (what is to be identified as) the critical point, fragmentation is limited to a relatively small number of miniscule fragments (largely monatomic and biatomic; Tables 1-3). Thus, the damage is relatively small and diffused, the extent of fragmentation is rather symbolic and the projectile is arrested (at a time designated t_A) distorted—to the various degree depending of the impact energy—but with retained integrity (Figure 1a). This (subcritical) velocity regime is *the damage phase* of the system, where the mass of the projectile stump is practically equal to the initial mass of the projectile ($m_{st} \approx m$).

Figure 1. *Snapshot of two severely deformed configurations of a projectile* $\bar{d} = 57$ *(m = 26047; the total mass given in number of atoms) following an impact at (a)* $v_i = 0.465$ *km/s and (b)* $v_i = 0.475$ *km/s. (a) The arrested projectile with no large fragments; the corresponding snapshot time exceeds the effective arrest time approximately three times (*$\approx 3 \cdot t_A$*). Note the nucleation of diffuse voids and initiation of nanoscale cracks by their coalescence. (b) The separation of the two largest fragment (followed by the projectile arrest shortly after) with notable growth of a blunted vertical crack whose propagation is stopped eventually. (The projectile stumps are cut to emphasize the proximal-end details. The stump disappears with the complete projectile fragmentation which is, within the present simulation framework, roughly identified with the striking velocity range of 2-3 km/s (Mastilovic, 2015). Furthermore, to get a feeling for the striking velocities used in the present investigation, the velocity of longitudinal elastic wave propagation of the LJ solid used herein is approximately 4.3-4.4 km/s which is within 5-10% of the reported values for tungsten (Mastilovic, 2016).)*

At very low striking velocities the plastic distortion at the proximal end of the projectile is accommodated by dislocation glide along favorably oriented planes (~30° with respect to the impact direction; Mastilovic and Krajcinovic, 1999). With increase of striking velocities, extensive atomic rearrangements occur with dominant damage mechanisms being void nucleation, growth and coalescence typical of ductile fracture (e.g., Besson, 2010). It is interesting to note that the relative shortening of the projectile obtained in MD simulations is in excellent agreement with the Taylor's classic analytical result (1948) as demonstrated already by Mastilovic and Krajcinovic (1999).

The simulation data suggest that the onset of non-negligible fragmentation is—depending on the projectile diameter—in the broad interval of (0.47–0.56) km/s, which can be, consequently, identified with the incipient fragmentation velocity interval (that is, the critical velocity range). At this finite-size-dependent critical striking velocity, $v_c(d)$, the fragment distribution is still rather limited to miniscule fragments: the overwhelming majority is monatomic up to four-atom clusters (Table 1). The most notable difference compared to the subcritical response is an ejection of *a pair* of large fragments (corresponding roughly to the $0.1 \cdot m$ for the aspect ratio, $\lambda \approx 7.5$, used herein) illustrated in Figure 1b and Table 1. The break-up of these two large fragments is an outcome of an extensive lateral mass transfer by massive atomic rearrangements

resulting in void nucleation/coalescence and slipping along the favorably oriented planes, which are operable on (sub)nanosecond timescale under the nanoscale size constraints.

This subjective, qualitative, and, therefore, rather arbitrary initial estimate of the incipient fragmentation velocity based on the mass of the largest fragment is quantitatively characterized by a transparent investigation approach based on the average fragment mass, which is used extensively in the recent computational fragmentation studies (Behara et al., 2005; Carmona et al., 2008; Sator et al., 2008; Timár et al., 2012).

Table 1. *Frequency distribution of fragment size n (in number of atoms constituting a fragment) for three striking velocities for $\bar{d} = 53$ (m = 22523) in the immediate D-F transition neighborhood with the range of data divided into the class intervals of equal width in the logarithmic space. Note that the largest cluster corresponding to the arrested projectile (the stump) is not included.*

		v_t [km/s]		
		0.465	**0.470**	**0.475**
$\ln n = 0$	$n = 1$	344	618	603
$0 < \ln n \le 1$	$n = 2$	16	38	22
$1 < \ln n \le 1.5$	$2 < n \le 4$	8	8	9
$1.5 < \ln n \le 2$	$4 < n \le 7$	0	0	0
$2 < \ln n \le 2.5$	$7 < n \le 12$	0	0	0
$2.5 < \ln n \le 3$	$12 < n \le 20$	0	0	0
$3 < \ln n \le 3.5$	$20 < n \le 33$	0	0	0
$3.5 < \ln n \le 4$	$33 < n \le 54$	0	1	0
$4 < \ln n \le 4.5$	$54 < n \le 90$	0	0	0
$4.5 < \ln n \le 5$	$90 < n \le 148$	0	0	0
$5 < \ln n \le 5.5$	$148 < n \le 244$	0	0	0
$5.5 < \ln n \le 6$	$244 < n \le 403$	0	0	0
$6 < \ln n \le 6.5$	$403 < n \le 665$	0	0	0
$6.5 < \ln n \le 7$	$665 < n \le 1096$	0	0	0
$7 < \ln n \le 7.5$	$1096 < n \le 1808$	0	2	2
$7.5 < \ln n \le 8$	$1808 < n \le 2981$	0	0	0

Damage-Fragmentation Transition

The sharp transition from damage to fragmentation in collision of solids is a fascinating phenomenon attracting a notable attention lately in physics literature (e.g., Kun and Herrmann, 1999; Åström et al., 2000; Carmona et al., 2008; Sator and Hietala. 2010; Timár et al., 2012). Kun and Herman (1999) demonstrated that the transition point between damaged and fragmented states behaved as *a critical point* and discussed the possible mechanisms of that continuous phase transition. They gave evidence that the strength of the largest fragment $\langle m_{\max}/m \rangle$ can be considered to be the order parameter of the D-F transition. (Hereinafter, the angle brackets $\langle \cdot \rangle$ designate the sample average and $m = N \cdot m_0$ the total projectile mass.) They also demonstrated that the transition point between the damaged and the fragmented phases can be identified with the maximum of the energy released normalized with the impact energy. Behara et al. in their computational study (2005) also associated the critical point with the impact velocity corresponding to the maximum value of the second largest fragment $(m_{\max}^{2nd})$ obtained from the impact fragmentation of a circular disc upon collision with a frictionless plate. Fortuitously or not, the critical point, $v_c = 0.47$ km/s, obtained in the present study for $\bar{d} = 53$ corresponds to the maximum value of $m_{\max}^{2nd}$ as indicated in Table 2.

Finally, Timár et al. (2010) argued that the threshold of the D-F transition can be identified not only with the curvature change of $m_{\max} = \hat{m}_{\max}(v_i)$ (Kun and Herrmann, 1999) but also with the striking velocity resulting in approximately comparable sizes of the largest ($m_{\max}$) and the second largest fragment $(m_{\max}^{2nd})$. For their simulation model of the impact fragmentation of 3D plastic particles this implies that one dominant crack propagates from the contact zone in the direction collinear with the striking velocity and splits the spherical impactor. It is interesting to note that—although the slender projectile used in the present impact fragmentation study has substantially different deformation, damage and failure patterns—the D-F phase transition can still be identified with surprising certainty with *the first* occurrence of two large fragments of similar size (Table 2).

Table 2. *Selected fragment statistics for seven striking velocities for $\bar{d} = 53$ with m = 22523. The largest cluster, corresponding to the arrested projectile (stump), is designated by m_{st} and the total number of fragments by n_F. Note that all mass values are given in number of atoms (of mass m_0) and the maximum temperatures (evaluated at two locations) in kelvin.*

	v_i [km/s]						
	0.425	**0.465**	**0.470**	**0.475**	**0.495**	**0.578**	**1.00**
m_{st}	22217	22122	18194	18622	18238	16016	8567
$m_{\max}$	3	4	1798	1715	1687	2016	1043
$m_{\max}^{2nd}$	2	3	1773	1507	1684	1152	814
m_{ave}	1.04	1.09	5.97	5.70	4.37	4.13	2.88
$T_{\max}$	2000/1100	2100/1200	2350/1100	2400/1100	2450/1250	2800/1500	5200/4000
n_F	295	368	667	636	847	1477	4376

Table 3. *Selected fragment statistics for seven striking velocities for $\bar{d} = 19$ with m = 2813.*

	v_i [km/s]						
	0.510	**0.555**	**0.560**	**0.565**	**0.646**	**0.800**	**1.00**
m_{st}	2736	2282	2173	2243	1883	1449	1159
$m_{\max}$	3	194	189	198	208	139	123
$m_{\max}^{2nd}$	3	147	138	187	143	93	62
m_{ave}	1.12	2.85	2.97	2.90	2.83	2.51	2.17
$T_{\max}$	2000/1300	2200/1300	2200/1400	2200/1400	2600/1400	3400/2500	4700/2900
n_F	86	185	213	213	320	536	758

Actually, out of ten projectile diameters used in the present computational study, the D-F threshold determined based on this qualitative criterion ($m_{\max}^{2nd} \approx m_{\max}$) agreed with the one determined based on the statistics of the average fragment mass (m_{ave}), in all cases but one. Nonetheless, even in the case of that exception (which was $\bar{d} = 19$, presented in Table 3) the critical striking velocities of the two citeria are within 5 m/s, which amounts to roughly 1% difference.

Finally, the average fragment mass was used most recently by Timár et al. (2012) for more transparent identification of the transition velocity in their 3D investigation of the impact fragmentation of spherical projectiles made of heterogeneous brittle materials by means of a discrete element model. This approach, which identifies the average fragment mass as the order parameter of the D-F phase transition, is adopted for this study as well. To put it succinctly, this method identifies the threshold value v_c as the striking velocity that coincides with the maximum of $m_{ave} = \hat{m}_{ave}(v_i)$. The average fragment mass is defined as the sample average of the ratio of the second and first moments of fragment masses

$$m_{ave} = \left\langle \frac{M_2}{M_1} \right\rangle \tag{1}$$

where the kth moment of the fragment distribution is defined in a single fragmentation event as

$$M_k = \sum_i m_i^k - m_{\max}^k, \quad (k = 1,2) \tag{2}$$

(Note that the summation is performed over all fragments m_i and the contribution of the maximum fragment mass is subtracted from M_k (Timár et al., 2012).) It cannot be overemphasized that, strictly speaking, the average mass (1) is defined as the sample average of the ratio of the first and the second moments of fragment masses over large number of realizations while—for the sake of computational tractability (in conjunction with the system sizes used in this study)—only a single realization is used throughout this analysis. This explains somewhat kinky, even serrated, character of the curves presented in Figure 2.

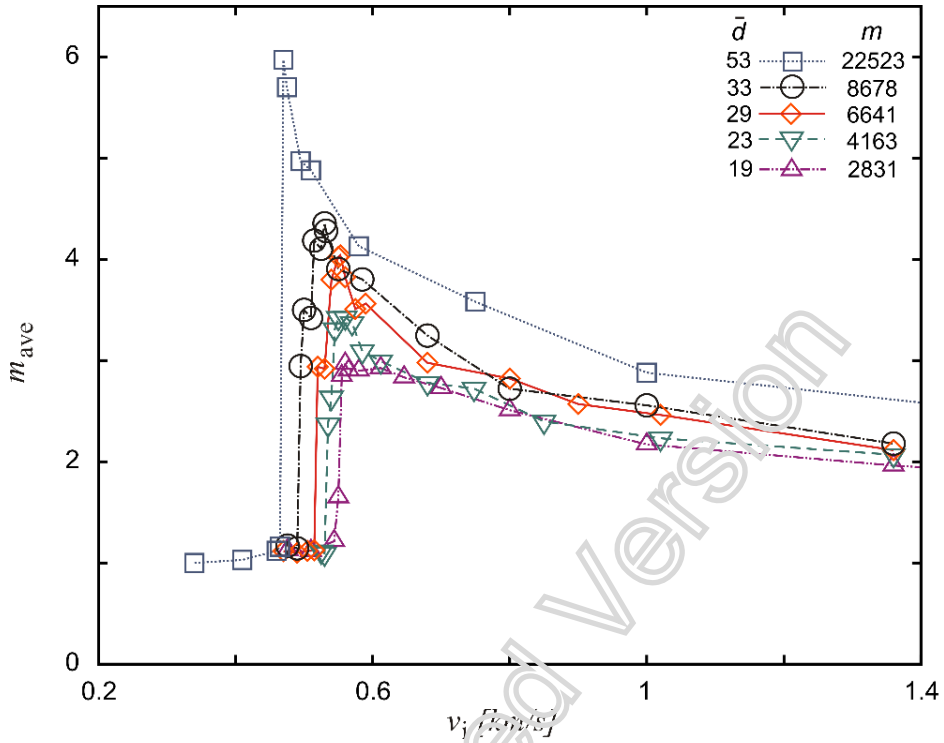

Figure 2. *Average fragment mass as a function of the striking velocity for five different projectile diameters of the same aspect ratio ($\lambda \approx 7.5$). (Note that with increasing system size the peak of the curves gets sharper and shifts to the lower v_i values as typically observed for continuous phase transition (Kun and Herrmann, 1999; Åström et al., 2000; Timár et al., 2012).*

The processed simulation results presented in Figure 2 reveal dependence of the average fragment mass (obtained in the abovementioned manner) upon the striking velocity for five different projectile diameters. The critical behavior for the largest projectile can be clearly observed due to the precipitous surge of the average fragment mass. The gradual smoothing of the $m_{ave} = \hat{m}_{ave}(v_i)$ curves following the projectile diameter decrease is clearly visible as well. The similar increase of sharpness of conditional moments with increase of the model size was observed by Campi (1988) in connection with the phase transition in nuclear multifragmentation. As for the impact fragmentation, Kun and Herrmann (1999) observed this critical-point signature behavior for the average fragment mass, Åström et al. (2000) for the total fragment mass, while Timar et al. (2012) for both the average fragment mass and the evolution rate of the scalar damage parameter.

The simulation data presented in Tables 2 and 3 also include the maximum values of the instantaneous kinetic temperature (Hoover, 1985; Holian, 1995) evaluated locally at two circular averaging areas (of equal radii $9 \cdot r_0$) positioned along the projectile centerline (refer to (Mastilovic, 2015, 2016) for details). Specifically, the first averaging area is centered in the proximal end while the second is in the mid-section, approximately at $0.2 \cdot l$ and $0.45 \cdot l$ from the projectile's impacting flat top, respectively (l being the projectile length defining the aspect ratio as $\lambda = l/d$). (The second T_{max} value is also—in the pre-fragmentation phase—a reasonably close estimate of the steady-state temperature established in the projectile stump after the thermal equilibration.) The maximum temperature data pairs indicate that the D-F transition is not accompanied by a significant increase in the atomic vibratory motion defining the instantaneous kinetic temperature. Actually, in the D-F transition region, the maximum temperature increases approximately 10% which is relatively modest change for the calculation accuracy of ±50K.) The substantial temperature rise occurs with the increase in the level of fragmentation well above the critical point.[2]

Finally, the total number of fragments, n_F, presented in Tables 2 and 3 is an important measure of the degree of break-up of the fragmenting impactor (Behara et al., 2005; Sator and Hietala, 2010). It is observed in the present study that the maximum average mass (identified in the following analysis with the critical state) results from simultaneous occurrence of a pair of large fragments of comparable size *accompanied* by as small as possible "dust cloud" of monatomic fragments. It is important to note that it is difficult to reach the steady state n_F in MD simulations since the shock induced heating yields extreme temperatures that can dissipate only through heat transfer to the projectile stump. This process of thermal equilibration of the arrested projectile takes a long time and even after the uniform temperature is reached—depending on the impact energy—its steady-state value can be sufficiently large to cause occasional atom escape. Consequently, the emission of monatomic fragments due to the thermal vibratory motion remains for some time after the projectile arrest.

Furthermore, the present simulation results (Figure 3) support the conclusion by Behara et al. (2005) that the number of fragments scales linearly with the natural logarithm of the striking velocity normalized by the critical striking velocity

[2] It has been recently demonstrated that, within the present MD simulation framework, the maximum fragment size is inversely proportional to the maximum value of the instantaneous kinetic temperature within a large part of the hypervelocity impact range ($3 \text{ km/s} \leq v_i \leq 30 \text{ km/s}$) (Mastilovic, 2015).

$$n_F \propto \ln\left(\frac{v_i}{v_c}\right), \quad v_c < v_i < v_L \tag{3}$$

It is interesting to note that, based on the large-projectile data presented in Table 2, the total number of fragments raises notably in the D-F phase transition range, which is not surprising since the emission of a large number of miniscule fragments (overwhelmingly monatomic; Mastilovic (2015)) always accompanies the large fragment brake-off due to the shock induced thermal excitation. Consequently, it appears that the total number of fragments, n_F, could also be considered a candidate for the D-F transition order parameter.

It should also be emphasized that n_F necessarily diverges from the elucidated linearity of the scaling relation (3) for ultra-high striking velocities approaching the terminal (shattering) fragmentation

$$\lim_{v_i \to v_1}(n_F) = N \tag{4}$$

where $N = m / m_0$ is the total number of atoms constituting the monoprojectile and v_1, the elusive shattering transition velocity (Mastilovic, 2015). Thus, the fragmentation process asymptotically approaches the terminal fragmentation defined by a deterministic fragment distribution following from the monatomic sample of fragments ($m_{max} \equiv 1$). According to Figure 3, the striking velocity v_L, corresponding to this divergence from linearity of the scaling expression (3), is size sensitive with values 10 km/s and 30 km/s corresponding approximately to the normalized projectile diameters 19 and 53, respectively. The later limit value agrees rather well with the earlier observations suggesting linear scaling of the maximum fragment mass with a set of state variables in the lower and intermediate part of the hypervelocity impact range (Mastilovic, 2015).

Interestingly, Sator and Hietala (2010), in their investigation of damage in the impact fragmentation of 2D circular discs, proposed a linear relation

$$D_f \propto n_F \tag{5}$$

between the final damage and the total number of fragments, with an obvious consequence that the process defined by Eq. (4) corresponds to the approach to the limit damage state, $D_f = 1$. The importance of this proposition stems from the fact that, unlike the evaluation of the total number of fragments, the experimental measurement of damage evolution remains a challenging problem (Tasan et al., 2012; Saijun et al., 2014; Iturrioz et al., 2014), especially the dynamic ductile damage quantification.

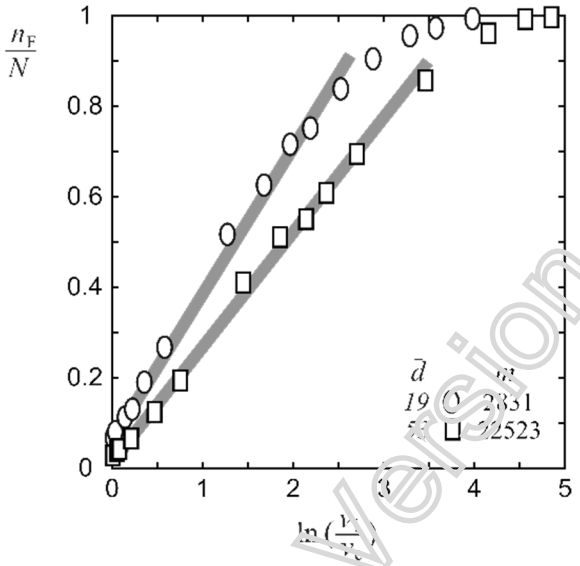

Figure 3. *The total number of fragments normalized by the number of atoms vs. natural logarithm of the striking velocity normalized by the critical velocity at two projectile diameters presented in Tables 2 and 3.*

Size Effect of the Damage-Fragmentation Transition Threshold

The dependence of the critical striking velocity on the slender projectile's diameter is illustrated in Figure 4. It can be noticed that the central part of this plot corresponds to the power-law decrease.

Assuming the well-known scaling form (Stauffer and Aharoni, 1992; Nishimori and Ortiz, 2011; Timar et al., 2012) for the critical striking velocity

$$v_c(d) = v_c(\infty) + A d^{-1/\nu}, \qquad d_l \le d \tag{6}$$

in terms of the system size, the critical striking velocity of the infinite system and the correlation length exponent of the transition can be identified to be $v_c(\infty) = 0.40$ km/s and $\nu = 0.77 \pm 0.01$,[3] respectively. Eq. (6)

[3] Timar et al. (2012) also observed this type of size effect for their spherical particle impacts with the exponent $\nu = 1.00 \pm 0.05$.

implies that in the limit of the very large projectiles the critical striking velocity of the D-F phase transition converges to $v_c(\infty)$. The present MD simulation results, on the other hand, suggest limits of applicability of the power law (6). Specifically, the entirely new feature of the functional dependence $v_c = f(d)$ is the existence of two horizontal plateaus corresponding to the small ($\bar{d} \leq \bar{d}_l = 23$) and, parhaps also, the large projectile diameters ($\bar{d} \geq \bar{d}_u = 57$).

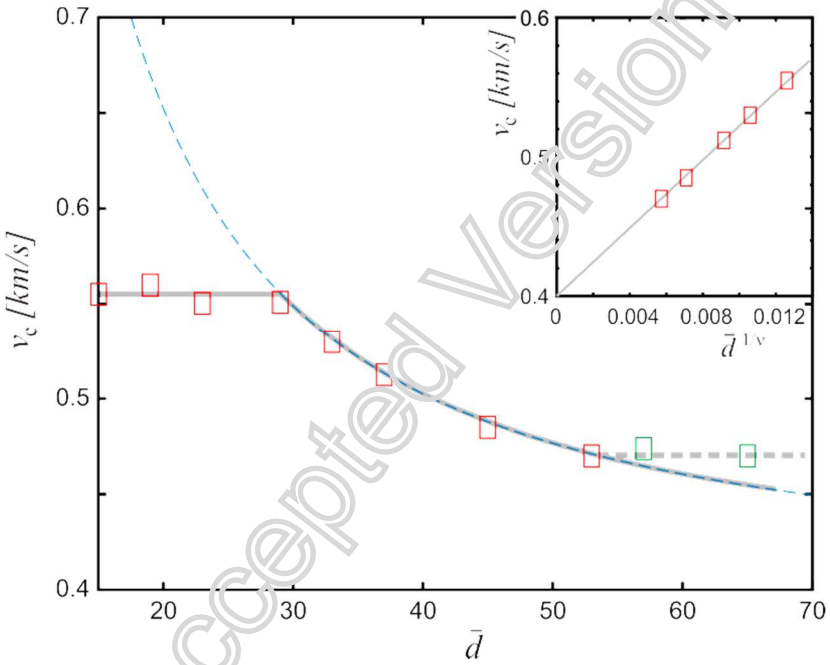

Figure 4. *Main panel: The critical value of the striking velocity as a function of the projectile diameter. Inset: The critical value of the striking velocity as a function of the projectile diameter raised to the degree $1/\nu = 1.30$ extracted in Eq. (6); the five indicated power-law data points outline the critical value of the impact velocity of infinite systems, $v_c(\infty) = 0.40$ km/s.*

The small-size saturation is actually suggested by the two smallest disc-radii data presented by Kun and Herrmann in their groundbreaking article ((1999); Figure 9) but the issue was not pursued. This saturation plateau is similar to the well-known size effects noticed in the plasticity of confined dimensions. The physical explanation of this marked sample-size dependent inelastic response is commonly attached to change in

deformation mechanisms when the system volume approaches the nanoscale. For example, Kraft et al. (2010) demonstrated the size dependency of the mechanical strength of different monocrystalline thin metal films and proposed that it may be separated into three regimes: the small-size regime, an intermediate regime governed by the power law, and a bulk-like regime. They argued that "there is no scaling law with one universal power-law exponent encompassing the entire range" since different physical mechanisms give rise to different inelastic responses for different size ranges (and boundary conditions). They supported this claim with observations of decreasing dislocation density and activity with decreasing film thickness resulting eventually in the dislocation starvation for the nanoscale samples. Similarly, Rinaldi et al. (2012) demonstrated effects of dislocation density and sample-size on the yield stress at the nanoscale in any plastic regime; Rinaldi (2011) casted the dependence mathematically into a first-order Weibull theory. Jennings et al. (2011) noticed the same trend that the size dependence of the compressive strength in monocrystalline Cu nanopillars deviates from "the ubiquitously observed power law" to a relatively size-independent upper plateau at the small-size end. They associated this change with the change in nanoplasticity mechanisms from the surface dislocation nucleation at the small diameters to the collective dislocation dynamics at the larger diameters in accordance with the theoretical predictions by Zhu et al. (2008). A similar trend of the strength increase due to the transition from cooperative to microcrack nucleation phenomena were discussed for quasi-brittle solids by Mastilovic (2011a, 2011b, 2013). While the small-size plateau analogs are well known and extensively discussed in the nanoscale plasticity in the last decade, the occurrence of the large-size saturation, observed in the present investigation, is unexpected at such, relatively small, (pre-bulk) sample volumes. This apparent large-tail saturation limit exceeds by 10-15% the critical velocity of the unbounded media (extracted from the inset of Figure 4). As an illustration, Eq. (6) suggests that the D-F phase transition for $\bar{d} = 57$ (m = 26047) should take place at v_i = 0.465 km/s. Nonetheless, Figure 1a shows that at the time corresponding to $3 \cdot t_A$ the arrested projectile retained completely its integrity for that striking velocity with a solid margin while at v_i = 0.470 km/s only one large fragment is ejected. The two large fragments occur for the first time at v_i = 0.475 km/s (Figure 1b), which is identified as the critical velocity based on the observation that the average fragment mass exceeds those obtained for v_i = 0.485, 0.510, 0.612 km/s. It can be argued that the difference between these two critical velocity values (suggested by Eq. (6), v_c = 0.465 km/s, and the maximum of $m_{ave} = \hat{m}_{ave}(v_i)$ method, v_c = 0.475 km/s) is reasonably small, but, the similar trend is also observed for the largest projectile used in this study ($\bar{d} = 65$, m = 33836) with a similar critical velocity

(Figure 4). Due to the scarcity of the large system size data and the lack of the clear physical explanation at present (other than, seemingly premature, identification of the large-size limit with the bulk behavior), the existence of the apparent large-size saturation limit at such, relatively small, size is an iffy proposition and the discussion must be relinquished to future studies.

Scaling of the Average Mass with the Projectile Diameter

The average fragment mass, Eq. (1), characterizes the fragment mass fluctuations (Stauffer and Aharoni, 1992; Kun and Herrmann, 1999; Timar et al, 2012). Consequently, assuming that the system exhibits a continuous phase transition, the finite size scaling of the average fragment mass in the form

$$m_{ave} = d^{\gamma/\nu} F\left\{\left[v_i - v_0(\infty)\right] d^{1/\nu}\right\} \tag{7}$$

(where F denotes the scaling function) reveals the γ exponent of the D-F phase transition. Figures 5 and 6, illustrate the data collapse of the $m_{ave} = \hat{m}_{ave}(v_i)$ curves for two values of the critical velocity of the unbounded media $v_c(\infty) = 0.40$ km/s and $v_c(\infty) = 0.43$ km/s, respectively. For both cases, the best collapse is achieved with the scaling exponent $\gamma = 1.04 \pm 0.02$. This exponent value significantly exceeds the one obtained by Timar et al. (2012) in their recent study of scaling laws for impact fragmentation of spherical solids based on 3D discrete element model.

Inset in Figure 5 reveals both the good quality data collapse of $m_{ave} = \hat{m}_{ave}(v_i)$ curves in the neighborhood of the critical point for the three selected projectile diameters $d \geq d_l$ as well as the horizontal peak shift of the curves belonging to the small size plateau $d < d_l$. A detail in the inset of Figure 5, with emphasized $\bar{d} \in \{19, 23\}$ curve peaks illustrate the horizontal peak shift of the curves belonging to the small size plateau in resemblance to the claim by Kraft et al. (2010) that there is no scaling law with one universal power-law exponent encompassing the entire size-dependent range (of the mechanical strength). Nonetheless, prompted by the unexpectedly early large-size $v_c = f(d)$ saturation illustrated in Figure 4, an attempt is made to scale the simulation data with somewhat larger critical velocity of unbounded media, $v_c(\infty) = 0.43$ km/s.

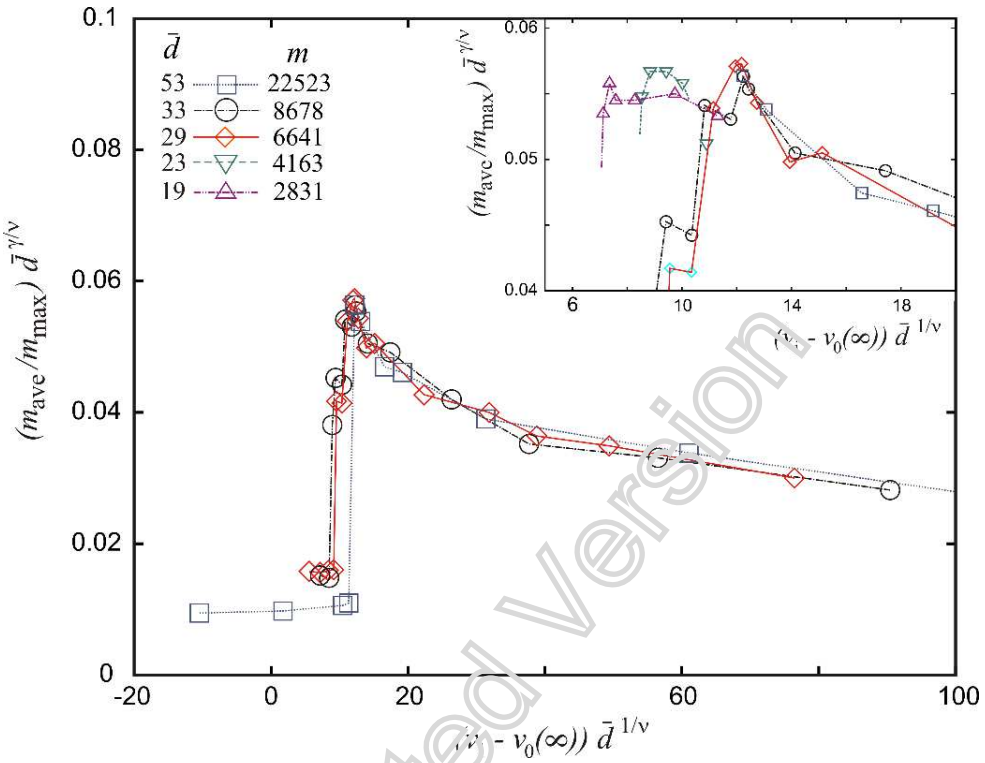

Figure 5. *Main panel: Collapse of the $m_{ave} - v_{ave}(v_i)$ curves presented in Figure 2 corresponding to three different projectile diameters ($\bar{d} \in \{29, 33, 53\}$ belonging to the power-law part of Figure 4) obtained by rescaling the average fragment mass, m_{ave}, and the striking velocity, v_i, by an appropriate power of the projectile diameter. Inset: A detail of the main panel plot corresponding to the peak of the curves with the data points $\bar{d} \in \{19, 23\}$ added for illustration of the horizontal peak shift of the curves belonging to the small size plateau.*

Regardless of reasonably good data collapse presented in Figure 6, a closer examination reveals a small—albeit, an indicative—scatter in the neighborhood of the critical point. This expected scatter is an unavoidable reflection of the earlier observation that data points for $\bar{d} \in \{19, 23\}$ do not follow the power-law scaling of the critical striking velocity (6).

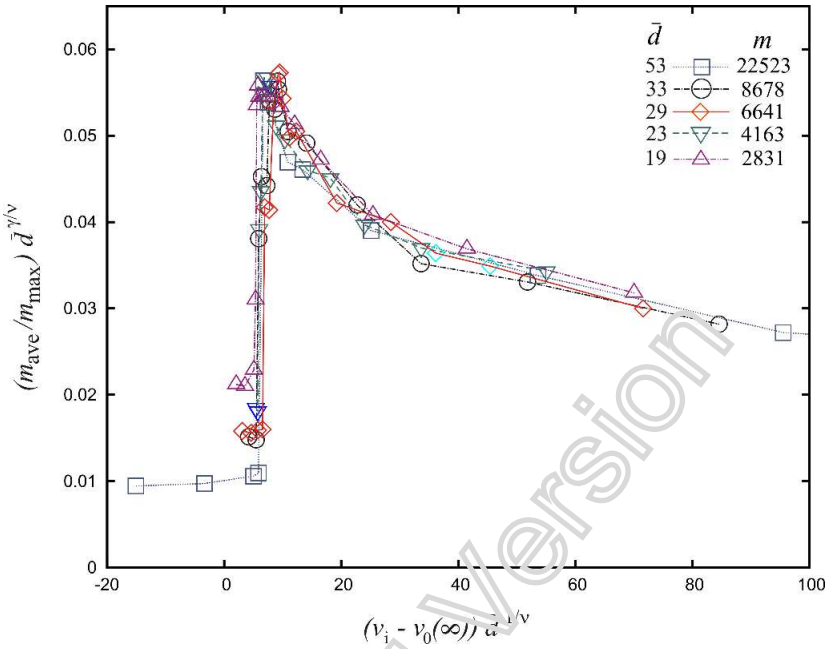

Figure 6. *Collapse of the* $m_{ave} = \hat{m}_{ave}(v_i)$ *curves presented in Figure 2 corresponding to five different projectile diameters obtained by rescaling the average fragment mass,* m_{ave}*, and the striking velocity,* v_i*, by the same scaling exponents of the projectile diameter and the increased impact velocity of infinite systems,* $v_c(\infty) = 0.43$ *km/s modified to take into account all simulation data points.*

SUMMARY

The current article presents a general model for 2D impact fragmentation of slender projectiles using the traditional MD. The principal advantage of this computational method is the ability to study rapid non-equilibrium processes with small-scale spatial and temporal resolutions with no assumptions made about the processes and mechanism investigated. Simulations are performed with slender rectangular projectiles of a fixed aspect ratio and 10 different diameters by varying the striking velocity within a relatively wide range of interest. It is well established nowadays that the impact fragmentation becomes critical at certain striking velocity, v_c (i.e., the impact energy). Thus, MD simulations are performed with a relatively moderate-energy loading of a slender monocrystalline nanoprojectile onto a rough rigid surface to explore D-F phase transition with emphasis on the size effects and scaling behavior. At first, the simulation results are used to explore the

dependence of selected fragment statistics upon the striking velocity. The rigid-anvil impacts for all striking velocities below the D-F transition ($v_i < v_c$) lead to more or less severe plastic distortion accompanied by a relatively small and diffuse nanoprojectile damage in the process zone but with notable absence of substantial fragmentation. At striking velocities exceeding this fragmentation threshold, the projectile is no longer capable of retaining its integrity by completely absorbing its kinetic energy by plastic distortion and, consequently, fragmentation takes place as a result of shear-dominating cracking typical of ductile solids.

The identification of the critical velocity is performed by the method based on the maximum average fragment size, commonly used in recent studies. This analysis suggests that the critical velocity varies in the interval of (0.47–0.56) km/s for the set of projectile sizes used herein. The occurrence of the maximum average fragment is a result of an interplay between large fragments and accompanying "dust cloud" of miniscule fragments, overwhelmingly monatomic. It is observed that, within the present simulation framework, the critical velocity coincides with the smallest striking velocity with sufficient impact energy to brake-off two "non-negligible" fragments of comparable size ($m_{\max}^{2nd} \approx m_{\max}$) with as small as possible size of accompanying "dust cloud". It is also reported that this D-F transition is accompanied with only a modest increase of the maximum temperature in the process zone and somewhat more pronounced increase or the total number of fragments which may suggest the latter for an order-parameter candidate.

Thus, assuming the scaling forms (6, 7), well-known from percolation theory and previous impact-fragmentation studies, the power-law scaling exponents are identified ($\nu = 0.77 \pm 0.01$ and $\gamma = 1.04 \pm 0.02$) as well as the critical striking velocity of the unbounded media ($v_c(\infty) = 0.40$ km/s), which define the dependence of the critical striking velocity and the average fragment mass upon the projectile diameter under the fixed aspect ratio constraint. Interestingly enough, the MD simulation results suggest existence of the lower limit of applicability ($d_p = 23\ r_0 \approx 6.5$ nm) of the critical striking velocity power law (6) and, perhaps, the upper one as well. It cannot be overemphasized, though, that the existence of these limits is not established herein with the same degree of confidence due to the fact that the MD simulations of the impact fragmentation of the larger systems are prohibitively time consuming, which results in the scarcity of data on that end of the size spectrum. Consequently, the existence of the small size plateau (perhaps a horizontal asymptote – it cannot be stipulated based on the data available) is well confirmed by the simulation results and well founded in the recent experimental and theoretical nanoplasticity studies. Namely, there is a plethora of experimental data on mechanical strength on the nanoscales published recently that support this general

trend. On the other hand, the large-size horizontal plateau is suggested by a less comprehensive set of simulation results, which highlights a shortcoming of the present, and an incentive for the future, work.

The use of the scaling form characteristic of continuous phase transition resulted in high-quality data collapse in a broad critical point neighborhood. The simulation results and the scaling analysis presented in this study extend the validity of the phase transition picture on the slender impactors and yield the D-F transition exponents with a reasonable accuracy.

Furthermore, the present simulation results demonstrate that the number of fragments scales linearly with the natural logarithm of the striking velocity normalized by the critical striking velocity until the upper linearity threshold is reached for ultra-high striking velocities approaching the terminal (shattering) fragmentation. This size-dependent limit velocity is roughly estimated to be $v_L \approx 30$ km/s for $\bar{d} = 53$.

Finally, the main limitations of the present MD model can be attributed to the modest size (up to 34000 atoms), the 2D geometry, and the rudimentary pairwise interatomic interactions. They are used to benefit from their simplicity and the consequent computational efficiency. Thus, the exponents in the scaling expressions, as well as their applicability limits, could change for 3D geometry. Unfortunately, due to the prohibitively costly increase of the simulation run time, the extension of the present modeling framework in that direction would require a substantially more sophisticated computing technology (in terms of both software and hardware) than the one used in the present study. (As an additional benefit, the 3D geometry would enable a realistic modeling of polycrystalline projectiles.) Furthermore, recommendations for future work include the use of interatomic potentials more physically justified for the modeling of complex systems; needless to emphasize, at the cost of further increase of the computational intensity. Nonetheless, the use of more realistic many-body potentials (as an example, the embedded atom model) would improve the fragmentation model and refine the simulation results especially in the range of low and moderate striking velocities inherent to the D-F transition. Additionally, it seems opportune to mention possibility of exploring presumably higher-order effects such as the initial temperature of the *solid* projectile and the pre-existing structural imperfections at various spatial scales (e.g., point defects, voids, inclusions) that would be associated with a relatively-insignificant additional computational cost. In the end, it would be interesting to make an assessment of the influence of the frictionless target on the results presented in this study, which would require only a simple source code modification without a consequent simulation run time increase.

ACKNOWLEDGMENT

The author acknowledges a partial financial support by the Ministry of Education, Science and Technological Development of the Republic of Serbia.

REFERENCES

Allen, M.P. and Tildesley, D.J. 1996. *Computer Simulation of Liquids*, Oxford University Press, Oxford.

Andrews, E.W. and Kim, K.-S. 1998. Threshold conditions for dynamic fragmentation of ceramic particles, *Mechanics of Materials* 29, 161-180.

Åström, J.A., Holian B.L., and Timonen J. 2000. Universality in Fragmentation, *Physical Review Letters* 84 (14), 3061-3064.

Behera, B., Kun, F., McNamara, S., and Herrmann, H.J. 2005. Fragmentation of a circular disc by impact on a frictionless plate, *Journal of Physics: Condensed Matter* 17, S2439–S2456.

Besson, J. 2010. Continuum Models of Ductile Fracture: A Review, *International Journal of Damage Mechanics* 19 (1), 3–52.

Buehler, M.J., 2008. Atomistic Modeling of Materials Failure, New York: Springer.

Campi, X. 1988. Signals of a phase transition in nuclear multifragmentation, *Physics Letters B* 208, 351-354.

Carmona, H.A., Wittel, F.K., Kun, F., and Herrmann, H.J. 2008. Fragmentation processes in impact of spheres, *Physical Review E* 77, 051302.

Chaikin, P.M. and Lubenski, T.C. 1995. Principles of the Condensed Matter, Cambridge: Cambridge University Press.

Diehl, A., Carmona, H.A., Araripe, L.E., Andrade Jr, J.S., and Farias, G.A. 2000. Scaling behavior in explosive fragmentation, *Physical Review E* 62, 4742-4746.

Dongarra, J.J. et al. 2008. Productivity Evaluation on Emerging Architectures. Advances in Computers, Vol. 72, High Performance Computing, ed. M.V. Zelkowitz. Academic Press

Herrmann, H.J., Wittel, F.K. and Kun, F. 2006. Fragmentation, *Physica A* 371, 59-66.

Holian, B.L. and Grady, D.E. 1988. Fragmentation by Molecular Dynamics: The Microscopic "Big Bang." *Physical Review Letters* 60 (14), 1355-1358.

Holian, B.L., Voter, A.F. and Ravelo, R. 1995. Thermostatted molecular dynamics: how to avoid the Tada demon hidden in Nose-Hoover dynamics, *Physical Review E* 52: 2338-2347.

Hoover, W.G., 1985. Canonical dynamics: Equilibrium phase space distributions, *Physical Review A* 31: 1695-1697.

Iturrioz, I., Lacidogna, G. and Carpintery, A. 2011b. Acoustic emission detection in concrete specimens: Experimental analysis and lattice model simulations, *International Journal of Damage Mechanics*, 23, 327-358.

Jennings, A.T., Li, J., and Greer, J.R., 2011. Emergence of strain-rate sensitivity in Cu nanopillars: Transition from dislocation multiplication to dislocation nucleation, Acta Materialia 59, 5627-5637.

Katsuragi, H., Sugino, D, and Honjo, H. 2003. Scaling of impact fragmentation near the critical point, *Physical Review E* 68, 046105.

Katsuragi, H., Sugino, D, and Honjo, H. 2004. Crossover of weighted mean fragment mass scaling in two-dimensional brittle fragmentation, *Physical Review E* 70, 065103(R).

Kraft, O., Gruber, P.A., Monig, R., Weygand, D. 2010. Plasticity in confined dimensions, *Annual Review of Materials Research* 40, 293-317.

Krajcinovic, D. 1996. Damage Mechanics, Amsterdam: Elsevier.

Kun, F. and Herrmann, H.J. 1999. Transition from damage to fragmentation in collision of solids. *Physical Review E* 59 (3), 2623-2632.

Mastilovic, S. 2011a. Some Observations Regarding Stochasticity of Dynamic Response of 2D Disordered Brittle Lattices, *International of Damage Mechanics*, 20, 267-277.

Mastilovic, S. 2011b. Further Remarks on Stochastic Damage Evolution of Brittle Solids Under Dynamic Tensile Loading, *International Journal of Damage Mechanics*, 20, 900-921.

Mastilovic, S. 2013. On strain-rate sensitivity and size effect of quasi-brittle solids: Transition from cooperative phenomena to microcrack nucleation. *Continuum Mechanics and Thermodynamics* 25, 489-501.

Mastilovic, S. 2015. Impact fragmentation of nanoscale projectiles at ultrahigh striking velocities, *Meccanica* 50, 2353-2367.

Mastilovic, S. 2016. Molecular-dynamics simulations of the nanoscale Taylor test under extreme loading conditions, *Mathematics and Mechanics of Solids* 21(3), 326-338.

Mastilovic, S. and Krajcinovic, D. 1999. Statistical models of brittle deformation: Part II: computer simulations, *International Journal of Plasticity* 15, 427-456.

Mastilovic, S. and Rinaldi, A. 2014. Two-Dimensional Discrete Damage Models: Discrete Element Methods, Particle Models, and Fractal Theories, 273-304; in *Handbook of Damage Mechanics: Nano to Macro Scale for Materials and Structures,* Ed. Voyiadjis G., Springer, Berlin.

Moukarzel, C.F., Silvia F. Fernández-Sabido, S.F., and J. C. Ruiz-Suárez, J.C. 2007. Phase transition in liquid drop fragmentation, *Physical Review E* 75, 061127.

Nishimori, H. and Ortiz, G. 2011. *Elements of Phase Transitions and Critical Phenomena.* Oxford University Press, Oxford.

Rinaldi, A. 2011. Effects of dislocation density and sample size on plastic yielding at the nanoscale: a Weibull-like framework, *Nanoscale* 3 (11), 4817-4823.

Rinaldi, A., Peralta, P., Sieradzki, K., Traversa, E., and Liccoccia, S. 2012. Role of Dislocation Density on the Sample-Size Effect in Nanoscale Plastic Yielding, Journal of *Nanomechanics and Micromechanics* 2(3), 42-48.

Saijun, Z., Chi, Z., Qinxiang, X., and Songmao, C. 2014. Measurement of full-field ductile damage based on resistance method, *Procedia Engineering* 81, 1055-1060.Sá Martins, J.S. and de Oliveira, P.M.C. 1998. Lattice Simulations in Nuclear Multifragmentations, *International Journal of Modern Physics C* 9, 867-874.

Sator, N., Mechkov, S., and Sausset, F. 2008. Generic behaviours in impact fragmentation, *European Physics Letters* 81, 44002.

Sator, N. and Hietala, H. 2010. Damage in impact fragmentation, *International Journal of Fracture* 163:101–108.

Stauffer, D. and Aharoni, A. 1992. *Introduction to Percolation Theory.* Taylor & Francis, London.

Tasan, C.C., Hoefnagels, J.P.M., and Geers, M.G.D. 2012. Identification of the continuum damage parameter: An experimental challenge in modeling damage evolution. *Acta Materialia* 60, 3581-3589.

Taylor, G., 1948. The use of flat-ended projectiles for determining dynamic yield stress. I. Theoretical considerations. *Proceedings of the Royal Society of London A* 194, 289-299.

Thornton, C, Yin, K.K., and Adams, M.J. 1996. Numerical simulation of the impact fracture and fragmentation of agglomerates, *Journal of Physics D: Applied Physics* 29, 424–435.

Timár, G., Blömer, J., Kun, F. and Herrman, H.J. 2010. Scaling laws for impact fragmentation of spherical solids. *Physical Review Letters* 104: 095502.

Timár, G., Kun, F., Carmona, H.A. and Herrmann, H.J. 2012. Scaling laws for impact fragmentation of spherical solids. *Physical Review E* 86 (4): 016113.

Verlet, L. 1967. Computer "Experiments" on Classical Fluids. I. Thermodynamics Properties of Lennard-Jones Molecules. *Physical Review* 159 (1), 98-103.

Wu, Y., Magallanes, M. and Crawford, J.E. 2014. Fragmentation and debris evolution modeled by a point-wise coupled reproducing kernel/finite element formulation. *International Journal of Damage Mechanics* 23 (7), 1005-1034.

Zhou, M. 2003. A new look at the atomic level virial stress: on continuum-molecular system equivalence, *Proceedings of the Royal Society of London A* 459: 2347-2392.

Zhu, T., Li, J., Samanta, A., Leach, A., and Gall, K. 2008. Temperature and Strain Rate Dependence of Surface Dislocation Nucleation, *Physical Review Letters* 100, 025502.